CHEMISTRY OF MATERIALS
Article

Chem. Mater. **2010,** *22,* 3943–3951 3943
DOI:10.1021/cm1005295

Electrochemical Codeposition of Thin Gold Nanoparticles/Sol−Gel Nanocomposite Films

Reut Toledano and Daniel Mandler*

Institute of Chemistry, The Hebrew University of Jerusalem, Jerusalem 91904, Israel

Received February 20, 2010. Revised Manuscript Received May 29, 2010

We present a new method for deposition of thin nanocomposite films made of sol−gel-based Au nanoparticles using a single electrochemical step. Applying a negative potential to an electrode (indium tin oxide or stainless steel) immersed in a solution of gold nanoparticles stabilized with *N*-[3-(trimethoxysilyl)propyl] ethylenediamine (EDAS) caused the reduction of the protic solvent, which altered the pH and therefore catalyzed the deposition. The nanocomposite thin films were characterized by various techniques: the morphology and structure of the layers were examined by high-resolution scanning electron microscopy and atomic force microscopy; their thickness was determined by profilometry; and the permeability of the films was studied by electrochemistry. We found that homogeneous defect-free layers could be deposited only upon adding tetramethoxysilane (TMOS) to the deposition solution. Furthermore, we showed that the applied potential, the ratio between the TMOS and the Au nanoparticles, and the type of the substrate significantly affected the aggregation and density of the Au nanoparticles in the nanocomposite. Finally, by applying a positive potential to the nanocomposite films we succeeded to electrochemically dissolve the embedded Au nanoparticles, forming holes and channels. The oxidation treatment had a remarkable effect on the permeability of the film and exposed the electrode to faradic activity. This method seems to be of general applicability in templating of nanometer-sized objects in thin films.

Introduction

Combining of nanoparticles with polymers to form nanocomposites opens the route for engineering materials with advantageous electrical, optical, and mechanical properties.[1−6] Recent advances in this field provide the means of exploiting the interactions between the two phases and thereby tune the macroscopic properties of the nanocomposites.[7]

One of the major obstacles for the commercialization of nanocomposites is the inadequacy of cost-effective methods for controlling the dispersion of the nanoparticles in the polymeric matrix. The nanoparticles often tend to aggregate within the polymer, which cancels out any benefits associated with their nanoscopic dimension. The interactions of nanoparticles with the matrix are governed by the stabilizing shell of the nanoparticles, which therefore affects their spatial distribution and behavior.[8] The polymeric matrix can prevent the oxidation and coalescence of the nanoparticles and increase the stability and durability of the nanocomposites. Hence, the uniqueness of polymer-based nanocomposites, as compared with other nano-objects, is in the influence of the matrix on the nanocomposite performance and matrix−nanoparticle interactions.[9]

Embedding of various nanoparticles within silicate-based matrices has been used in a number of technological applications, such as decorative coatings,[10] catalysis,[11] optical filters,[12] nonlinear optical materials,[13] and others.[14−22] Sol−gel processing offers a number of significant advantages

*Corresponding author. E-mail: mandler@vms.huji.ac.il. Fax: 972 2 6585319. Tel: 972 2 6585831.

(1) Bharathi, S.; Nogami, M.; Lev, O. *Langmuir* **2001**, *17*, 2602.
(2) Epifani, M.; Carlino, E.; Blasi, C.; Giannini, C.; Tapfer, L.; Vasanelli, L. *Chem. Mater.* **2001**, *13*, 1533.
(3) Bronstein, L. M.; Polarz, S.; Smarsly, B.; Antonietti, M. *Adv. Mater.* **2001**, *13*, 1333.
(4) Khushalani, D.; Hasenzahi, S.; Mann, S. *J. Nanosci. Nanotechnol.* **2001**, *1*, 129.
(5) Hayakawa, T.; Ono, Y.; Nogami, M. *Proc. SPIE* **2000**, *102*, 3943.
(6) Anderson, M. L.; Morris, C. A.; Stroud, R. M.; Merzbacher, C. I.; Rolison, D. R. *Langmuir* **1999**, *15*, 674.
(7) Ajayan, P. M.; Schadler, L. S.; Braun, P. V. *Nanocompos. Sci. Technol.* **2003**, 248.
(8) Balazas, A. C.; Emrick, T.; Russell, T. P. *Science* **2006**, *314*, 1107.
(9) Lee, L. J.; Zeng, C.; Cao, X.; Han, X.; Shen, J.; Xu, G. *Compos. Sci. Technol.* **2005**, *65*, 2344.
(10) Pothukuchi, S.; Li, Y.; Wong, C. P. *J. Appl. Polym. Sci.* **2004**, *93*, 1531.
(11) Weyl, W. A. *Coloured Glasses*; Society of Glass Technology: Sheffield, U.K., 1951.
(12) Braun, S.; Rappoport, S.; Zusmen, R.; Avnir, D.; Ottolenghi, M. *Mater. Lett.* **1990**, *10*, 1.
(13) Bohmer, M. R.; Balkenende, A. R.; Bernards, T. N. M.; Peeters, M. P. J.; van Bommel, M. J.; Boonekamp, E. P.; Verheijen, M. A.; Krings, L. H. M., Vroon, Z. A. E. P. In *Handbook of Advanced Electronic and Photonic Materials Devices*; Nalwa, H. S., Ed.; Academic Press: San Diego, 2001.
(14) Nogami, M.; Selvan, S. T.; Song, H. In *Handbook of Advances Electronic and Photoelectronic Devices*; Nalwa, H. S., Ed.; Academic Press, San Diego, 2001.
(15) Daniel, M.; Astruc, D. *Chem. Rev.* **2004**, *104*, 293.
(16) Katz, E.; Willner, I.; Wang, J. *Electroanalysis* **2004**, *16*, 19.
(17) Dai, X.; Wildgoose, G. G.; Salter, C.; Crossley, A.; Compton, R. G. *Anal. Chem.* **2006**, *78*, 6102.
(18) Chengs, W.; Dong, S.; Wang, E. *Anal. Chem.* **2002**, *74*, 3599.
(19) Menon, V. P.; Martin, C. R. *Anal. Chem.* **1995**, *67*, 1920.
(20) Moretto, L. M.; Pepe, N.; Ugo, P. *Talanta* **2004**, *62*, 1055.
(21) Ugo, P.; Moretto, L. M.; Vezza, F. *ChemPhysChem* **2002**, *3*, 917.

Published on Web 06/15/2010

as a matrix for encapsulating nano-objects: (1) the high porosity of the sol−gel matrix, e.g., silica, titania, and zirconia, allows high mass-transport between the nanoparticles and surrounding; (2) the optical properties of the nanoparticles are only slightly affected by the UV−visible transparent matrix; and (3) these nanocomposites may be readily cast in a variety of forms including monolith and thin films.[23−26]

Sol−gel technology enables to incorporate almost any type of nanoparticles. The formation of nanocomposites based on the entrapment of various nanoparticles into sol−gel matrix has been reviewed and discussed.[27−31] The incorporation of semiconducting, metallic, ferroelectric, or scintillating nanoparticles in various oxide matrices has been reviewed by Mackenzie et al.[32] Gold and silver nanoparticles incorporated in sol−gel are probably the most studied systems. For example, Lev and co-workers successfully demonstrated the sol−gel encapsulation of metal nanoparticles in silicates.[33] The incorporation of metallic nanoparticles into a sol−gel matrix has been utilized in electrochemical sensing. For example, Ramaraj et al. designed an amperometric sensor with highly dispersed gold nanoparticles in a sol−gel film for H_2O_2 sensing without immobilizing a mediator or enzyme.[34] Liz-Marzan et al.[23] described a procedure for the homogeneous incorporation of silica-coated gold nanoparticles within transparent silica gels. They showed, based on the UV−vis absorption spectra and transmission electron microscopy, that there was no aggregation of the metal nanoparticles during sol−gel transition. Wei and co-workers presented a facile synthesis of mesoporous gold-silica nanocomposites through one-step sol−gel reactions of tetraethoxysilane with gold sol in the presence of dibenzoyl tartaric acid as a nonsurfactant template.[35]

Electrochemical deposition is an appealing approach for preparing nanoparticles due to its simple and low-cost implementation. By electrochemically reducing metal ions in an electrolyte solution, growth of a variety of different sizes and shapes of nanostructured particles has been obtained on metal,[36,37] semiconductor,[38,39] and polymer surfaces.[40]

The electrochemical codeposition of nanocomposites has been reported although not exhaustively studied.[41−57] Walcarius electrodeposited silica films on gold electrodes in order to detect Cu(II) in water−alcohol solutions.[57] Zhitomirsky reviewed the various strategies for the fabrication of nanostructured organic−inorganic films using electrophoretic deposition.[56] In his review, he summarized different approaches whereby polyelectrolytes, e.g., poly(ethylene imine), were electrochemically codeposited with metal ions as well as with ceramic nanoparticles. The electrochemical codeposition of carbon nanotubes/conducting polymers has also been demonstrated.[42−45,47,50] Other studies involved the electrochemical codeposition of oxide and metal nanoparticles, such as Ni, in primarily inorganic matrices, e.g., Al_2O_3.[46,52] A dominant organic matrix, which has been used for the electrochemical formation of nanocomposites, is chitosan.[41,48,49] For example, Zhou et al. reported the preparation of Cu_2O/chitosan nanoparticles by electrochemical deposition of nanocrystalline Cu_2O onto chitosan nanoparticles,[54,55] whereas Chen proposed an electrochemical deposition method for the formation of a chitosan−carbon nanotube nanocomposite for assembling an electrochemical biosensor.[48]

We present here a different and new approach where nanoparticle/sol−gel nanocomposites were prepared in a single electrochemical step. Specifically, the electrochemical codeposition of thin nanocomposite films made of sol−gel and embedded gold nanoparticles was accomplished by applying a negative potential to a solution consisting of a sol−gel precursor and gold nanoparticles stabilized with *N*-[3-(trimethoxysilyl)propyl] ethylenediamine (EDAS). The nanocomposites were characterized by a number of surface techniques including high-resolution scanning electron microscopy, atomic force microscopy, and transmission electron microscopy. We find that the

(22) Szamocki, R.; Reculusa, S.; Ravaine, S.; Bartlett, P. N.; Kuhn, A.; Hempelmann, R. *Angew. Chem., Int. Ed.* **2006**, *45*, 1317.
(23) Kobayashi, Y.; Correa-Duarte, M. A.; Liz-Marzan, L. M. *Langmuir* **2001**, *17*, 6375.
(24) De, G. *J. Sol−Gel Sci. Technol.* **1998**, *1*, 289.
(25) Scott, B. J.; Wirnsberger, G.; Stucky, G. D. *Chem. Mater.* **2001**, *13*, 3140.
(26) Bharathi, S.; Fishelson, N.; Lev, O. *Langmuir* **1999**, *15*, 1929.
(27) Innocenzi, P.; Brustain, G.; Martucci, A.; Urabe, K. *Thin Solid Films* **1996**, *279*, 23.
(28) Hench, L. L.; Valentine, J. K. *Chem. Rev.* **1990**, *90*, 33.
(29) Dave, B. C.; Dunn, B.; Valentine, J. S.; Zink, J. I. *Anal. Chem.* **1994**, *66*, 1120A.
(30) Sampath, S.; Lev, O. *Adv. Mater.* **1997**, *5*, 410.
(31) Bharathi, S.; Lev, O. *Anal. Commun.* **1998**, *35*, 29.
(32) Mackenzie, J. D.; Bescher, E. P. *Acc. Chem. Res.* **2007**, *40*, 810.
(33) Bharathi, S.; Joseph, J.; Lev, O. *Electrochem. Solid-State Lett.* **1999**, *6*, 284.
(34) Maduralveeran, G.; Ramaraj, R. *J. Electroanal. Chem.* **2007**, *608*, 52.
(35) Cheng, S.; Wei, Y.; Feng, Q. W.; Qiu, K. Y.; Pang, J. B.; Jansen, S. A.; Yin, R.; Ong, K. *Chem. Mater.* **2003**, *15*, 1560.
(36) Nichols, R. J.; Schroer, D.; Meyer, H. *Electrochim. Acta* **1995**, *40*, 1479.
(37) Tremont, R. J.; Cruz, G.; Cabrera, C. R. *J. Electroanal. Chem.* **2003**, *558*, 65.
(38) Stiger, R.; Craft, B.; Penner, R. M. *Langmuir* **1999**, *15*, 790.
(39) Gorer, S.; Ganske, J. A.; Hemminger, J. C.; Penner, R. M. *J. Am. Chem. Soc.* **1998**, *120*, 9584.
(40) Ortega, J. M. *Thin Solid Films* **2000**, *360*, 159.
(41) Pang, X.; Zhitomirsky, I. *Surf. Coating Technol.* **2008**, *202*, 3815.
(42) Fang, F. F.; Choi, H. J.; Joo, J. *J. Nanosci. Nanotechnol.* **2008**, *8*, 1559.
(43) Tsai, Y. C.; Hong, Y. H. *J. Solid State Electrochem.* **2008**, *12*, 1293.
(44) Gajendran, P.; Saraswathi, R. *Pure Appl. Chem.* **2008**, *80*, 2377.
(45) Chen, Q.; Zhao, L.; Li, C.; Shi, G. Q. *J. Phys. Chem. C* **2007**, *111*, 18392.
(46) Wei, X. Y.; Prewett, P. D.; Jiang, K. *2007 IEEE Conference on Nanotechnology*; Hong Kong, Aug 2−5, 2007; IEEE: Piscataway, NJ, 2007; p 34−38
(47) Baibarac, M.; Gomez-Romero, P. *J. Nanosci. Nanotechnol.* **2006**, *6*, 289.
(48) Luo, X. L.; Xu, J. J.; Wang, J. L.; Chen, H. Y. *Chem. Commun.* **2005**, *16*, 2169.
(49) Pang, X.; Zhitomirsky, I. *Mater. Chem. Phys.* **2005**, *94*, 245.
(50) Lu, S. Y.; Lin, I. H. *J. Phys. Chem. B* **2003**, *107*, 6974.
(51) Shao, I.; Vereecken, P. M.; Cammarata, R. C.; Searson, P. C. *J. Electrochem. Soc.* **2002**, *149*, C610.
(52) Peipmann, R.; Thomas, J.; Bund, A. *Electrochem. Acta* **2007**, *52*, 5808.
(53) Lepiller, C.; Poissonnet, S.; Bonnaillie, P. *J. Electrochem. Soc.* **2004**, *151*, D13.
(54) Chen, J. Y.; Zhou, P. J.; Li, J. L. *Carbohydr. Polym.* **2008**, *72*, 128.
(55) Chen, J. Y.; Zhou, P. J.; Li, J. L. *Carbohydr. Polym.* **2007**, *67*, 623.
(56) Zhitomirsky, I. *J. Mater. Sci.* **2006**, *41*, 8186.
(57) Walcarius, A.; Sibottier, E. *Electroanalysis* **2005**, *17*, 1716.

applied potential as well as the ratio between the gold nanoparticles and sol−gel monomer (not attached to the Au NPs) greatly affected the size and morphology of the gold nanoparticles embedded in the sol−gel matrix. The removal of the gold nanoparticles was achieved by their anodic dissolution, hence creating templated pits that were imaged by atomic force microscopy. Electrochemistry of these pitted thin films proved that oxidation of the gold nanoparticles exposed the electrode to faradic activity.

Experimental Section

Instrumentation. Electrochemical experiments were performed with a VersaStat potentiostat (EG&G) using a standard three-electrode cell with an Ag/AgBr wire as a reference electrode and a 6 mm diameter graphite rod as a counter electrode. The working electrodes were indium tin oxide (ITO) on glass (CG-60IN-CUV, $R_S = 15-25\ \Omega$, Delta Technologies Stillwater, MN) or 316 L stainless steel (SS) plates. A homemade lifter was used to withdraw the substrates from the deposition solutions at a rate of ca. 50 μm s^{-1} while constantly applying the potential and with slow stirring.

Scanning electron microscopy (SEM) images were acquired with a JEOL JSM-6400 microscope using an electron-beam intensity of 5 keV. Analysis of the elements in the SEM measurements was performed with energy-dispersive X-ray analysis (EDX). The thickness of the deposited films was measured with a profilometer (P-15, KLA-Tencor Co., San Jose, CA). The size of the nanoparticles was determined with Zetasizer Nano Series (Malvern Instruments). Atomic force microscopy (AFM) and scanning tunneling atomic force microscopy (TUNA) measurements were carried out using a Nanoscope Dimension 3100 scanning probe microscope equipped with a Nanoscope IVa controller (Veeco). A magnetic etch silicon probe (MESP) was used in the AFM measurements while a tapping etch silicon probe (TESP) was used for the TUNA measurements.

Chemicals. Tetramethoxysilane (TMOS) and *N*-[3-(trimethoxysilyl)propyl]ethylenediamine (EDAS), $HAuCl_4$, and $NaBH_4$ were purchased from Aldrich (98% purity) and used as received. Absolute ethanol (AR, Frutarom), extra-pure KNO_3 (Merck), KCl, KH_2PO_4, HCl, hexaammineruthenium(III)chloride, and deionized water (EasyPure UV, Barnstead) were used for preparing the different solutions. Gold nanoparticles stabilized by EDAS were prepared following Lev at al. procedure.[58] Namely, EDAS was dissolved in 0.1 M KH_2PO_4 to which $HAuCl_4$ was added. HCl was added to this solution. The final concentrations of EDAS, $HAuCl_4$, and HCl were 10, 1, and 0.1 M, respectively. Formation of gold nanoparticles was achieved by adding dropwise 0.1 M $NaBH_4$.

Procedures. ITO or SS plates were washed prior to film deposition with deionized water, ethanol, and again with deionized water, followed by drying at room temperature for 1−2 h (SS electrode were polished with emery paper, 4000 grits, Buehler, before washing). 0.1 M KNO_3 was added to the gold nanoparticles solution. Several experiments were carried out after adding TMOS to the gold nanoparticles followed by hydrolysis under continuous stirring for 1 h at room temperature. The working electrodes were placed in the electrochemical cell and mounted on the lifter. Cyclic voltammetry (CV) was carried out (0 to −1 V vs Ag/AgBr) to determine the potential to be used for electrochemical deposition. Then, a constant negative potential was applied to the working electrode (−0.8 to −1.2 V vs Ag/AgBr) under continues stirring for 2 or 10 min. The current as a function of time was recorded. After this period, the electrode was slowly withdrawn under constant speed using the lifter while the potential was still applied, in order to obtain homogeneous films. The electrode was dried in air for 24 h before further characterization was performed. Profiles of the deposited sol−gel were recorded across a notch that was manually scratched by a wooden stick immediately after film deposition.

The electroactivity of the nanocomposite films was examined by CV using a solution of 1 mM $Ru(NH_3)_6^{3+}$ and 0.1 M KCl. Oxidation of the Au nanoparticles embedded in the nanocomposites was carried out by recording first a CV (0 to −0.4 V vs Ag/AgBr) in 0.1 M KCl and then applying a constant potential of 1.0 V vs Ag/AgBr for different durations. The films were inspected by SEM, AFM, and TUNA without any further treatment besides sputtering a thin Au/Pd film on a cross-section prior to imaging by SEM.

Results and Discussion

The induced electrochemical deposition of thin sol−gel films by altering the pH on the electrode surface has been used by us[59−62] and others[48,49,63−72] to deposit primarily different silica, titania and zirconia films. For example, Walcarius et al. showed that it was possible to induce ordering in the electrochemical deposition of silica by adding a surfactant to the solution.[73] More recently, we have shown that this concept could be used for the codeposition of electroreducible metals, e.g., copper, and sol−gel.[62] Yet, to the best of our knowledge, the codeposition of sol−gel and nanoparticles using this approach has never been reported. Hence, we decided to synthesize Au nanoparticles according to a known procedure[58] that are stabilized by an aminosilane precursor and attempted to electrochemically deposit these nanoparticles by applying a negative potential.

Specifically, Au nanoparticles were prepared by dissolving $AuCl_4^-$ in a solution of N-[3-(trimethoxysilyl)propyl]-ethylenediamine (EDAS) and reduced by $NaBH_4$. The nanoparticles showed a typical plasmon band at 520 nm.

(58) Bharathi, S.; Lev, O. *Chem. Cmmun.* **1997**, 2303.
(59) Shacham, R.; Avnir, D.; Mandler, D. *Adv. Mater.* **1999**, *11*, 384.
(60) Shacham, R.; Avnir, D.; Mandler, D. *J. Sol−Gel Sci. Technol.* **2004**, *31*, 329.
(61) Shacham, R.; Mandler, D.; Avnir, D. *Chem.—Eur. J.* **2004**, *10*, 1936.
(62) Toledano, R.; Shacham, R.; Avnir, D.; Mandler, D. *Chem. Mater.* **2008**, *20*, 4276.
(63) Collinson, M. M.; Higgins, D. A.; Kommidi, R.; Campbell-Rance, D. *Anal. Chem.* **2008**, *80*, 651.
(64) Collinson, M. M.; Maryanne, M. *Acc. Chem. Res.* **2007**, *40*, 777.
(65) Deepa, P. N.; Kanungo, M.; Claycomb, G.; Sherwood, P. M. A.; Collinson, M. M. *Anal. Chem.* **2003**, *75*, 5399.
(66) Collinson, M. M.; Moore, N.; Deepa, P. N.; Kanungo, M. *Langmuir* **2003**, *19*, 7699.
(67) Lui, L.; Hu, J. M.; Zhang, J. Q.; Cao, C. N. *Anal. Chem.* **2009**, *81*, 3199.
(68) Hu, J. M.; Liu, L.; Zhang, J. Q.; Cao, C. N. *Prog. Org. Coat.* **2007**, *58*, 265.
(69) Liu, L.; Hu, J. M.; Zhang, J. Q.; Cao, C. N. *Electrochim. Acta* **2006**, *52*, 538.
(70) Hu, J. M.; Liu, L.; Zhang, J. Q.; Cao, C. N. *Electrochim. Acta* **2006**, *51*, 3944.
(71) Liu, S. M.; Qian, X. L.; Xiao, J. Z. *J. Sol−Gel Sci. Technol.* **2007**, *44*, 187.
(72) Liu, S. M.; Xing, C. S.; Qian, X. L.; Xiao, J. Z. *Rare Met. Mater. Eng.* **2008**, *37*, 486.
(73) Walcarius, A.; Sibottier, E.; Etienne, M.; Ghanbaja, J. *Nat. Mater.* **2007**, *6*, 602.

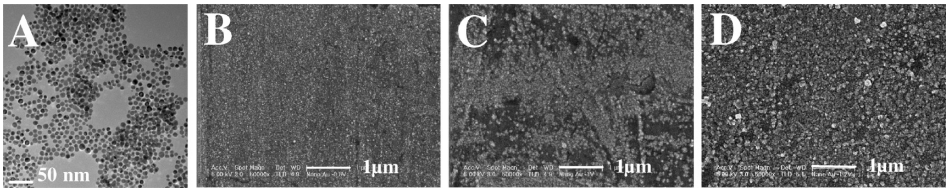

Figure 1. (A) TEM image of EDAS/Au NPs. SEM images (the bar indicates 1 μm) of EDAS/Au NPs nanocomposite film electrodeposited on SS plate as a result of applying different negative potentials: (B) −0.8, (C) −1, and (D) −1.2 V.

Table 1. Atomic Percentage of the Different Elements in the Deposited Films Obtained from EDX Analysis, As a Function of the Applied Potential (time of deposition was 10 min)

	applied potential (V)		
	−0.8	−1	−1.2
Si	2.8	3.0	3.4
Au	2.9	4.7	6.3
C	15.8	18.6	21.4
N	5.9	5.7	6.1
O	15.7	18.3	18.2
Fe	41.2	33.6	31.6

The average size of the nanoparticles determined by light scattering was 7.1 ± 0.5 nm. Analysis of the Au nanoparticles by TEM imaging (Figure 1A) yielded an average size of 6.4 ± 0.8 nm. Films were electrochemically deposited on ITO and stainless steel (SS) plates by applying a constant potential for different durations. The potential was determined from the CV (see Figure S1 in the Supporting Information) that was performed in the deposition solution prior to applying a constant potential. The cathodic current started to increase at potentials more negative than −0.8 V. Therefore, the applied potentials were defined by this potential and limited by the potential that caused visible hydrogen evolution. Figure 1B−D shows the effect of the applied potential on the morphology of the deposited films. EDX analysis, vide infra, confirmed that the nanometric deposits were made of gold and verified the presence of silica. It can be seen that as the potential was made more negative more gold nanoparticles deposited, which coagulated and formed larger deposits. This can be attributed to increasing the rate of solvent (ethanol) reduction, which increased the pH locally on the electrode surface and therefore accelerated the deposition of the silica-functionalized gold nanoparticles.

Table 1 summarizes the atomic percentage of the elements, i.e., silicon, gold, carbon, nitrogen, oxygen, and iron, in the deposited film (obtained from the EDX analysis) at different applied potentials. The analysis was carried out on a relatively large area (approximately 100 × 100 μm) that included many grains. It can be seen that as the applied potential was more negative, the percentage of the deposited gold, silicon and carbon increased, while that of iron decreased. These changes can be explained by an increase in the film thickness as the potential was more negative. The electron beam penetrated less into the underlying SS substrate as the film thickened. We cannot provide a simple explanation for the insensitivity of nitrogen to film thickness, yet it is known that the determination of nitrogen by EDX is somewhat problematic. A deeper inspection of the atomic percentage reveals that the ratio between

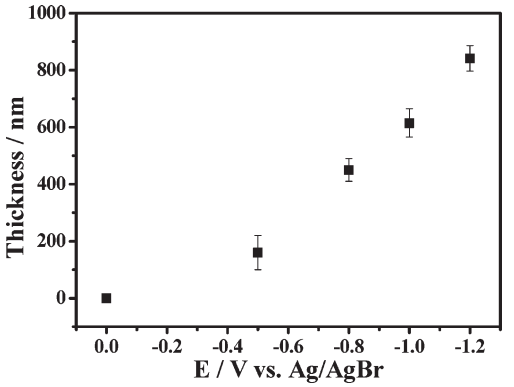

Figure 2. Thickness of the deposited films on a SS plate as a function of the applied potential. Time of deposition was 10 min.

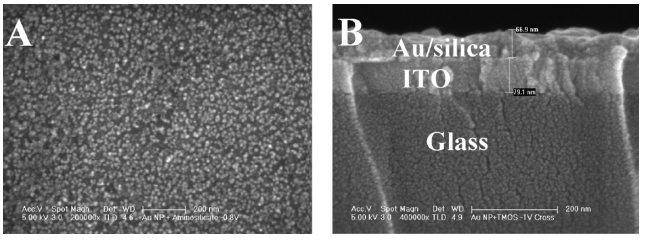

Figure 3. (A) SEM image (the bar indicates 200 nm) of EDAS/Au NPs nanoaomposite on an ITO substrate. (B) Cross-section of A, the thicknesses of the Au/silica film and the ITO layer are 67 and 79 nm, respectively. The applied potential was −1 V and time of deposition was 10 min.

silicon and nitrogen fits quite well with the expected 0.5 value, whereas the ratio between carbon and silicon increases from its expected value, i.e., 5 to approximately 6.4. We believe that as the film thickened the amount of entrapped solvent increased. It should be noted that the atomic percentage of gold cannot be straightforward compared with the other elements because of the dispersion of the nanoparticles on the surface.

Figure 2 shows the dependence of the film thickness on the applied potential. It is evident that electrochemical deposition commences at potentials that are more negative than ca. −0.5 V. Furthermore, it seems that the thickness of the electrochemically deposited films increases linearly from this threshold potential. As the applied potential becomes more negative the rate of hydroxyl generation increases which is the driving force for film deposition. These findings are in accordance with Brinker and Scherer's polymerization rate that is of first order with [OH^-].[74] Namely, the current (due to water reduction) varies almost

(74) Brinker, C. J.; Scherer, G. W.; Roth, E. P. *J. Non-Crystalline Solids* **1985**, *72*, 345.

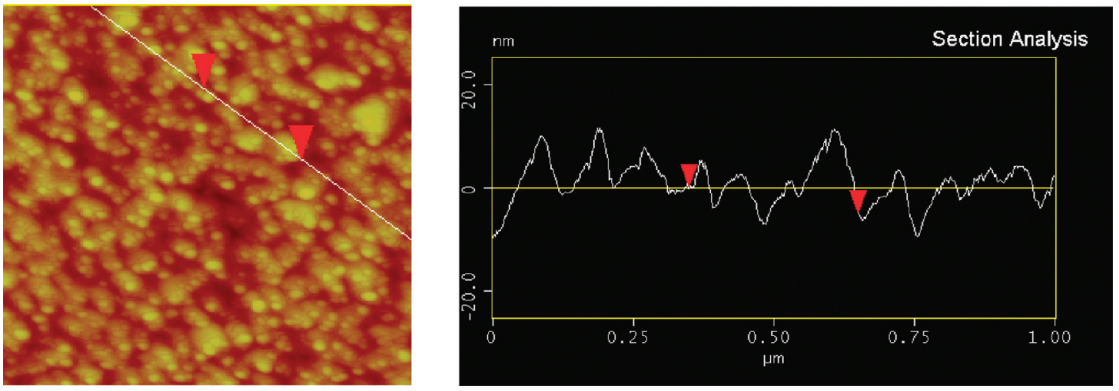

Figure 4. Tapping mode image ($1 \times 1\ \mu m^2$) and cross-section of EDAS/Au NPs nanocomposite electrochemically deposited by applying potential of −0.8 V for 10 min on an ITO substrate.

linearly with the applied potential (from the CV), which suggests that the concentration of hydroxyl ions at the electrode surface, and therefore the thickness of the deposited films, also varies linearly with potential.

The electrochemical deposition of gold nanoparticles in EDAS matrix is not limited to stainless steel and could basically be applied by a wide variety of electrode materials. Yet, envisaged applications are in the field of photonics and therefore most of our work was conducted using ITO substrates. Figure 3A shows a SEM image of EDAS/Au NPs nanocomposite electrochemically deposited on an ITO plate. A cross-section of the film is also shown (Figure 3B). The image shows that the ITO is entirely covered by a thin layer of gold nanoparticles embedded in the matrix. EDX analysis (see Table S1 in the Supporting Information) confirmed that the thin layer was made of silica and gold. It can be seen from Figure 3B that the coating is uniform and dense, and its thickness is approximately 70 nm.

AFM measurements were carried out in order to disclose the morphology of the surface. Figure 4 shows the AFM image of the EDAS/Au NPs nanocomposite and its cross-section. The Z-scale of the image is 50 nm and the imaging area is $1 \times 1\ \mu m$. It can be seen that a dense layer was obtained and the height average of the gold nanoparticles is less than 20 nm. It is worth mentioning that the size of a single nanoparticle cannot be determined by AFM from the lateral scale due to the high density of the particles that does not allow the AFM tip to penetrate in between the particles. The phase imaging (see Figure S2 in the Supporting Information) indicates that the layer consists of two distinct components.

Cyclic voltammetry (CV) was also employed for characterizing the films (Figure 5). Hexaammineruthenium(III)chloride was used as a redox probe for studying electron transfer across the film. The CV clearly shows that deposition of the EDAS/Au NPs nanocomposite does not block electron transfer. It can be seen that as the potential of deposition was more negative, the oxidation−reduction currents of the redox probe increased, although remained somewhat smaller than the bare ITO electrode. The reversibility of $Ru(NH_3)_6^{3+/2+}$ was not affected by the presence of the films. These results were

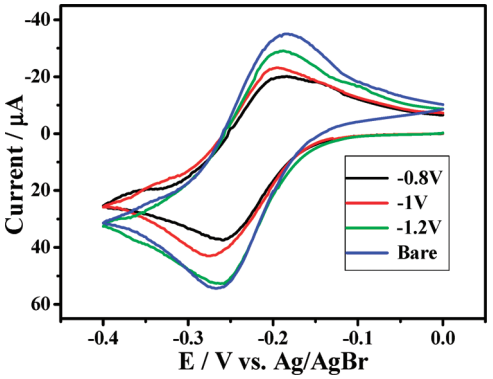

Figure 5. CV of 1 mM hexaammineruthenium(III)chloride in 0.1 M KCl recorded with bare and EDAS/Au NP nanocomposite ITO electrodes coated by applying different potentials for 10 min. Scan rate is 20 mV s^{-1}.

unexpected if the layers were uniform and defect-free. In spite of the fact that the gold nanoparticles are highly conducting their organo-silica shell and the interparticle distance would have blocked electron transfer. Moreover, in this case, the thicker the layers the smaller would have been the current. Therefore, our results suggest that electron transfer occurs not through the Au nanoparticles but on the ITO surface. This implies that the layers are inhomogeneous and are likely to possess defects, such as cracks.

The fact that higher currents are recorded as the deposition potential was more negative (resulting in thicker films) indicates that the density of defects increases respectively, presumably due to hydrogen evolution.

Tunneling atomic force microscopy (TUNA) is a scanning probe technique, which provides simultaneously conductivity and topography images with very high lateral resolution. Figure 6 shows the (A) topography and (B) conductivity of an electrochemically deposited EDAS/Au NPs nanocomposite film. The imaging area was $10 \times 10\ \mu m^2$, although smaller areas were also examined. We found that the conductivity of the covered areas was extremely low and only those areas that were not covered (and therefore are deeper in the topographic images) showed much higher conductivity that is attributed to the exposed ITO. Hence, the conducting areas in Figure 6B fully correlate with the dark spots in Figure 6A, leading to the conclusion that the film is indeed cracked. Moreover, there was no detectable

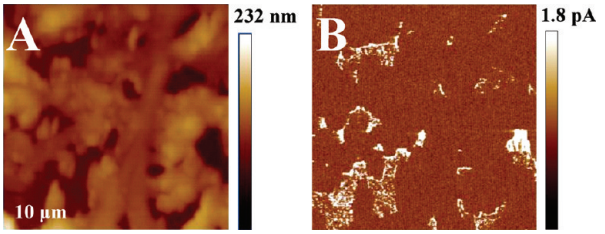

Figure 6. (A) Topography and (B) conductivity images of the nanocomposite film that was obtained by TUNA electrochemically by applying −1 V for 10 min.

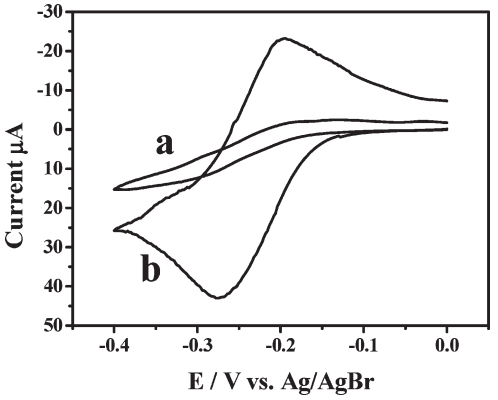

Figure 7. CV of EDAS/Au NPs nanocomposite (a) with and (b) without the addition of TMOS to the deposition solution. All other parameters are as in Figure 6.

difference in the conductivity of the film, which suggests that the Au nanoparticles are not ohmically connected to the underlying ITO.

All these findings indicate that the EDAS/Au NP nanocomposite films are inhomogeneous and have many defects. Therefore, TMOS was added to the deposition solution to fill the cracks and improve the uniformity of the layer. The solution containing TMOS- and EDAS-stabilized Au nanoparticles (1:1 mol/mol) was hydrolyzed while stirring for 1 h at room temperature followed by applying negative potential to an ITO surface. Figure 7 shows the CV of $Ru(NH_3)_6^{3+}$ recorded with ITO electrodes that were modified by EDAS/Au NPs nanocomposite with and without the addition of TMOS. It is clear that electron transfer was considerably blocked as a result of adding TMOS to the deposition solution implying that a significantly more uniform layer was obtained. TUNA imaging (not shown) revealed a completely isolated film, which is in accordance with the CV measurements.

SEM images of the layers are shown in Figure 8. The layers were deposited at −0.8 V for 10 min and the molar ratio between TMOS and EDAS/Au NPs was unity. It can be seen that the addition of TMOS resulted in the dilution of the Au nanoparticles in the nanocomposite film. The effect of the ratio between TMOS and the nanoparticles in the deposition solution will be discussed in the following section (see Figure 9 below).

Table 2 displays the atomic percentage of the elements in the electrochemically deposited films shown in Figure 8. The results confirm that the addition of TMOS to the deposited solution increases the atomic percentage of silicon,

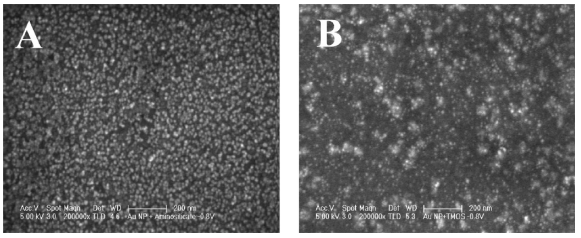

Figure 8. SEM images (the bar indicates 200 nm) of EDAS/Au NPs nanocomposites (A) with and (B) without the addition of TMOS deposited on ITO as a result of applying negative potential of −0.8 V for 10 min.

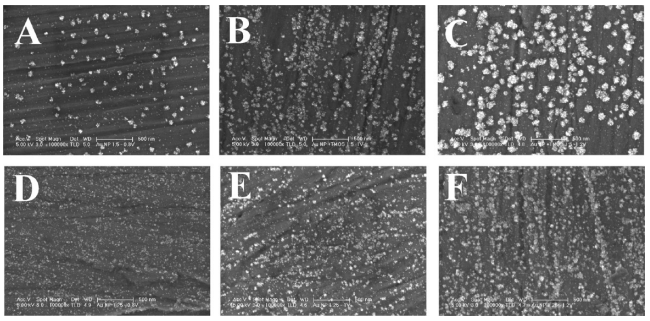

Figure 9. SEM images (the bar indicates 500 nm) of EDAS/Au NP nanocomposites on SS with the addition of TMOS employing different TMOS: EDAS/Au NP ratio [(A−C) 1:5, (D−F) 1:25] and various deposition potentials [(A, D) −0.8, (B, E) −1.0, and (C, F) −1.2 V]. Time of deposition was always 10 min.

Table 2. Atomic Percentage of the Different Elements (measured by EDX) in the Electrochemically Deposited Sol−Gel Films[a]

	TMOS and EDAS/Au	EDAS/Au
Si	13.5	4.9
Au	2.1	5.7
C	13.6	7.7
N	9.0	8.5
O	41.8	37.1
In	18.0	34.8

[a] "EDAS/Au" refers to a solution containing only the EDAS-stabilized Au NPs, whereas "TMOS and EDAS/Au" refers to the EDAS-stabilized Au NP solution to which TMOS was added (1:1 mol/mol ratio). Time and potential of deposition was as in Figure .

carbon, and oxygen, whereas the amount of gold decreases. Furthermore, the atomic percentage of indium (originating from the substrate) decreases, meaning a thicker film was deposited. Evidently, the electrochemical deposition of TMOS is more facile than that of the nanoparticles.

The control over the composition of the electrochemically deposited films can be achieved through the potential of deposition as well as the ratio between the two codeposited components. Figure 9 shows SEM images of stainless steel surfaces coated at different potentials and molar ratios between EDAS/Au NPs and TMOS. Figure 9A−C represents films with 1:5 TMOS:EDAS/Au ratios, whereas the ratio in Figure 9D−F was 1:25. The potential of deposition varied between −0.8 to −1.2 V. It can be seen that in accordance with the above results (Figure 1B−D), as the applied potentials was more negative (for both ratios), more gold nanoparticles deposited, aggregated, and formed larger deposits. Comparing the films deposited at

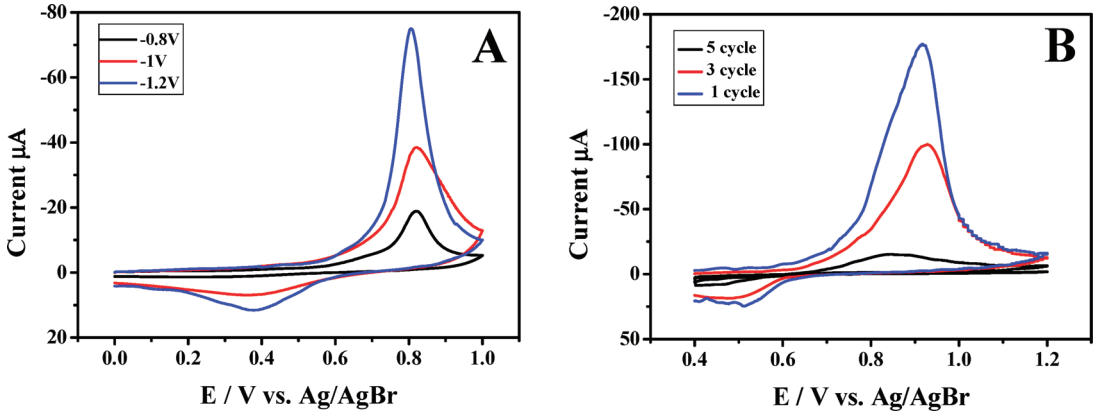

Figure 10. (A) CV of ITO electrode coated with EDAS/Au NPs nanocomposite film in 0.1 M KCl; (B) 1st, 2nd, and 5th CV of an ITO electrode coated at −0.8 V with EDAS/Au NPs. Time of nanocomposite deposition was 2 min and scan rate of CV was 20 mV s^{-1}.

two different TMOS:EDAS/Au NPs ratios, it is evident that the addition of smaller amounts of TMOS to the deposition solution resulted in denser films, i.e., the number of Au NPs per volume, with smaller aggregates. EDX analysis (see Table S2 in the Supporting Information) supports these observations. Namely, the atomic percentage of Si and C increased with the amount of TMOS added, whereas that of Au and Fe decreased. Furthermore, shifting the deposition potential to more negative values enhances the deposition of the Au NPs and at the same time resulted in thicker films.

The presence of Au in the nanocomposites can also be verified and quantified by electrochemistry. Positive potential was applied in order to locally oxidize and dissolve the gold nanoparticles. Apparently, deposition of the nanocomposites for 10 min caused the films to be overly thick, which made it impossible to electrochemically oxidize the embedded Au nanoparticles. Hence, deposition was shortened to 2 min resulting in the formation of thinner films. Figure 10A shows the oxidation of the films, which were deposited at various potentials. The anodic wave at 0.8 V is indicative of gold oxidation and the shape of the wave clearly points to a surface confined process. The reduction wave at 0.4 V is assigned to the reduction of $AuCl_4^-$ and suggests that the removal of gold is not very fast and therefore some gold can be redeposited by electrochemical reduction. It can be seen that as the applied potential (during deposition of the films) was more negative, the oxidation/reduction waves become larger. These results are with accordance with EDX analysis (Table 1). Figure 10B shows the first, second, and fifth CVs of an ITO electrode coated with EDAS/Au NPs (potential and time of deposition were −0.8 V and 2 min, respectively and the scan rate was 20 mV s^{-1}). It is apparent that the removal of Au from the film cannot be accomplished within one cycle and therefore we applied a constant potential (chronoamperometry) of 1.0 V for 10 min. This removed most of the gold, yet a few nanoparticles can still be detected after applying such positive potential by SEM. We believe the gold nanoparticles that remained intact were those that were not ohmically connected to the ITO surface. We estimate that the thickness of these films were ca. 100 nm, which means that most of the Au NPs were not directly

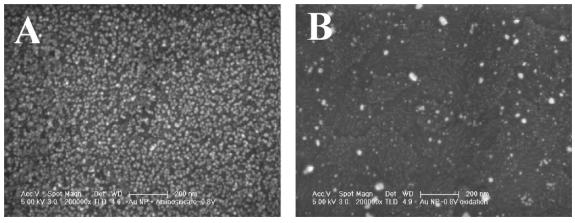

Figure 11. SEM images (the bar indicates 200 nm) of an ITO electrode coated with EDAS/Au NPs nanocomposite (A) before and (B) after applying 1.0 V for 10 min. The potential and time of deposition were −0.8 V and 2 min, respectively.

attached to the ITO surface. Yet, most of them were oxidized and removed, which suggests that their oxidation occurred by electron transfer through the NPs.

To confirm the oxidation and dissolution of the gold nanoparticles, we performed SEM measurements before and after the oxidation (Figure 11). A potential of 1.0 V was applied for 10 min. Comparison of the film before and after oxidation clearly shows the disappearance of most of the Au NPs. The film was examined in several places and the results were similar. EDX analysis (performed over 100 × 100 μm, see Table S3 in the Supporting Information) supports the visual inspection. Namely, the atomic percentage of all the elements besides Au did not change due to the oxidation of the films. The atomic percentage of Au decreased significantly from ca. 5 to 1%, independent of the potential at which the film was deposited.

The permeability of the films toward ionic species was examined by carrying out CV of $Ru(NH_3)_6^{3+}$ in 0.1 M KCl. Figure 12 shows the effect of the deposition potential on the behavior of this redox species. TMOS/EDAS Au NPs nanocomposites were deposited under different potentials for 2 min (Figure 12A). Furthermore, the CV of a dip-coated ITO electrode, which was immersed into the deposition solution for the same time, is also shown. It can be seen that faradic activity is observed in the dip-coated electrode, implying that a continuous homogeneous film was not deposited. On the other hand, as the applied potential was more negative a thicker film was obtained, which blocks more efficiently electron transfer across the interface. The sigmoid shape of the CVs of the electrochemically coated electrodes alludes to the existence

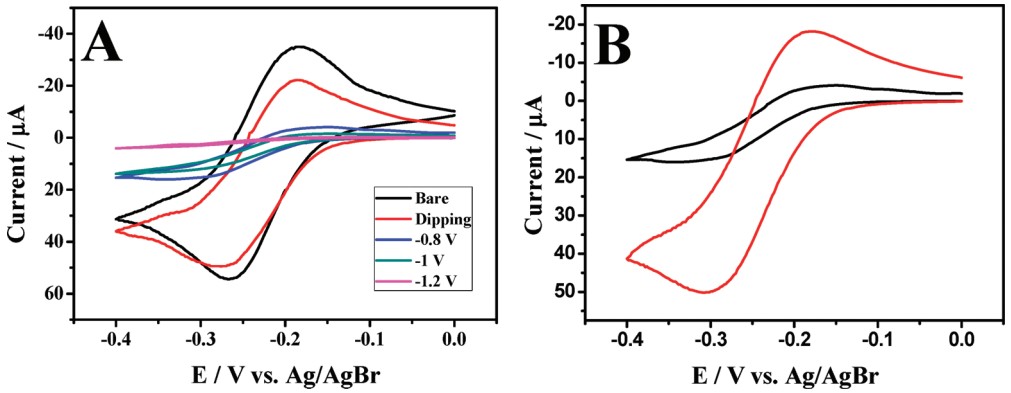

Figure 12. CV of 1 mM hexaammineruthenium(III)chloride in 0.1 M KCl. (A) ITO coated with TMOS and EDAS/Au NPs (1:1 ratio) by either applying different negative potentials for 2 min or by dip coating. (B) CV of an ITO-coated film (potential of deposition was −0.8 V) before (black line) and after (red line) applying 1.0 V for 10 min. Scan rate was 20 mV s^{-1}.

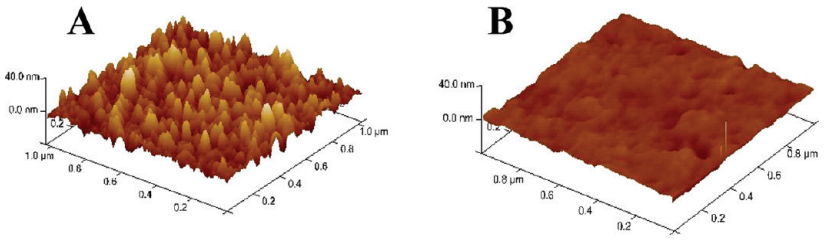

Figure 13. 3D AFM tapping mode images of ITO coated with EDAS/Au NPs nanocomposites (deposited at −1.0 V for 2 min) (A) before and (B) after oxidation (1.0 V for 10 min) of the Au nanoparticles.

of highly dispersed pinholes, which behave as micro or nanoelectrodes.[75] Deposition potential of −1.2 V yielded almost complete blocking of the ruthenium complex.

The oxidation of the Au nanoparticles had a remarkable effect on the permeability of the film as is shown in Figure 12B. It is evident that the oxidation and dissolution of the Au NPs opens channels in the film, which allows the facile diffusion of the redox species across the layer. The significant increase of the faradic current and the shape of the CV, which is characteristic of linear diffusion, are typical for a bare electrode. This is not surprising, as the density of the Au NPs in the original film (Figure 12A) is very high and their removal would leave similar density of holes or channels. This trend is independent of the potentials and time of deposition.

AFM measurements were carried out in order to confirm the formation of holes or channels following the oxidation of the Au nanoparticles. Images A and B in Figure 13 show AFM images of the layers before and after oxidation of the Au NPs (1.0 V for 10 min). The 3D tapping mode images (1×1 μm^2) clearly show the formation of holes as a result of Au oxidation. These findings are in accordance with our electrochemistry results, which proved the permeability of the film after the gold NPs oxidation. The roughness factor of the surface changed from 6.36 nm before to 1.32 nm after oxidation, which implies that the nanoparticles extrude significantly above the surface. The phase mode of AFM (see Figure S3 in the Supporting Information) becomes much more uniform after oxidation in comparison with the image before oxidizing the Au NPs.

Conclusions

The electrodeposition of sol−gel-based gold nanoparticles has been demonstrated by a single electrochemical step that resulted in thin nanocomposite films. Applying a negative potential to the electrode caused the reduction of the protic solvent, altered the pH and catalyzed the deposition of the gold nanoparticles embedded into the sol−gel matrix. The deposition was carried out on either ITO or stainless steel and represents a generic approach of coating conducting surfaces by nanocomposites. Characterization of the films by electrochemistry and tunneling atomic force microscopy revealed that the layers were inhomogeneous and possessed many defects. Therefore, tetramethoxysilane (TMOS) was added to the deposition solution to fill the cracks and improve the uniformity of the layer. We found a significant influence of primarily three parameters, i.e., the potential of deposition, the ratio of TMOS/Au NPs, and the type of the substrate on the structure and morphology of the deposits. In addition, we succeeded to electrochemically oxidize the embedded gold nanoparticles, which created holes and channels in the sol−gel matrix. AFM images acquired before and after the oxidation confirmed these results while electrochemistry showed that the electrochemical dissolution of the Au nanoparticles exposed the electrode surface to faradic activity and increased permeability of the film

(75) Wightman, R. M.; Wipf, D. O., *Electroanalytical Chemistry*; Bard, A. J., Ed.; Marcel Dekker: New York, 1989; Vol. *15*, p 267.

toward redox species. This approach is currently being examined as a means of imprinting nanoparticles in a matrix.

Acknowledgment. This study was supported by the Magnet project (Solar Energy Systems) and the Israel Science Foundation (Contract 85-06). The Harvey M. Krueger Family Center for Nanoscience and Nanotechnology of the Hebrew University is acknowledged.

Supporting Information Available: Additional material (PDF). This material is available free of charge via the Internet at http://pubs.acs.org.